Atmos. Meas. Tech. Discuss., 5, 3079–3115, 2012
www.atmos-meas-tech-discuss.net/5/3079/2012/
doi:10.5194/amtd-5-3079-2012

Atmospheric Measurement Techniques Discussions

A Cavity-Enhanced Differential Optical Absorption Spectroscopy instrument for measurement of BrO, HCHO, HONO and O_3

D. J. Hoch[1], J. Buxmann[1,3], H. Sihler[1,2], D. Pöhler[1], C. Zetzsch[3], and U. Platt[1]

[1]Institute of Environmental Physics, University of Heidelberg, Germany
[2]Max-Planck-Institute for Chemistry, Mainz, Germany
[3]Atmospheric Chemistry Research Laboratory, University of Bayreuth, Germany

Received: 28 March 2012 – Accepted: 10 April 2012 – Published: 26 April 2012

Correspondence to: D. J. Hoch (daniel.hoch@iup.uni-heidelberg.de)

Published by Copernicus Publications on behalf of the European Geosciences Union.

Abstract

The chemistry of the troposphere and specifically the global tropospheric ozone budget is affected by reactive halogen compounds like BrO or ClO. Bromine monoxide (BrO) plays an important role in the processes of ozone destruction, disturbance of NO_x and HO_x chemistry, oxidation of DMS, and the deposition of elementary mercury. In the troposphere BrO has been detected in polar regions, at salt lakes, in volcanic plumes, and in the marine boundary layer. For a better understanding of these processes instruments with high spatial resolution and high sensitivity are necessary. A Cavity Enhanced Differential Optical Absorption Spectroscopy (CE-DOAS) instrument was designed and applied. For the first time, such an instrument uses an UV-LED in the UV-wavelength range (325–365 nm) to identify BrO. In laboratory studies at the Atmospheric Chemistry Research Laboratory, University of Bayreuth, Germany, BrO, as well as HONO, HCHO, O_3, and O_4, could be reliable determined at detection limits (for five minutes integration time) of 20 ppt for BrO, 9.1 ppb for HCHO, 970 ppt for HONO, and 91 ppb for O_3, respectively. The best detection limits for BrO (11 ppt), HCHO (5.1 ppb), HONO (490 ppt), and O_3 (59 ppb) were achieved for integration times of 81 min or less.

1 Introduction

Besides their well known effects on stratospheric ozone, Reactive Halogen Species (RHS) are responsible for a series of phenomena in various compartments of the troposphere including volcanic plumes, coastal areas, salt lakes, and the polar boundary layer. For instance, RHS are of scientific interest, because they are mainly responsible for ozone depletion in the arctic boundary layer during polar spring. The phenomenon was first observed by Bottenheim et al. (1986), and several other studies followed e.g. Barrie et al. (1988, 1994); Bottenheim et al. (1990); Sturges et al. (1993); Kreher et al. (1997). The halogen catalyzed ozone depletion events occur only during polar sunrise. The release mechanism for reactive bromine is described by the "bromine

AMTD
5, 3079–3115, 2012

explosion" mechanism (Platt and Lehrer, 1996). The phenomenon is still not completely understood and is object of current research (Saiz-Lopez et al., 2007; Pöhler et al., 2010; Friess et al., 2011).

Also beside polar regions RHS strongly affect the ozone budget and the oxidation capacity of the atmosphere. Bromine monoxide (BrO) was detected in the mid-latitude marine boundary layer at different locations (Leser et al., 2003; Saiz-Lopez et al., 2004; Mahajan et al., 2010). At salt lakes high mixing ratios of BrO could be detected, up to 20 ppt at the Salar de Uyuni, Bolivia (Hönninger et al., 2004) and up to 220 ppt at the Dead Sea (Hebestreit et al., 1999; Matveev et al., 2001; Tas et al., 2008). Most of these observations were performed with LP-DOAS or MAX-DOAS measurement technique averaging over several kilometers. For a better understanding of the involved processes, measurements with high spatial resolution are essential, which can be achieved with mobile cavity based measurement techniques.

O'Keefe and Deacon (1988) started to use optical cavities with high reflective mirrors to observe absorbers by applying Cavity-Ringdown (CRD) spectroscopy. With this approach, the decay of light intensity leaking from the resonator after switching off the pump light source is measured. Since then the technique was continuously refined (Zalicki and Zare, 1995; Paldus et al., 2000; Ball et al., 2001; Fawcett et al., 2002; Simpson, 2003; Ball and Jones, 2003; Schuster et al., 2009). However most CRD have to avoid any absorptions beside that of the investigated trace gas for the used wavelength. This requires typically closed resonators with aerosol inlet filters. A second approach, the so-called Cavity Enhanced Absorption Spectroscopy (CEAS), was developed, which relies on measuring the transmittance of the resonator by recording the leak-out intensity (Engeln et al., 1998; Peeters et al., 2000). In contrast to CRDS the CEAS approach uses a continuous wave (CW) source of radiation. Based on CEAS, e.g. Fiedler et al. (2003); Langridge et al. (2006); Venables et al. (2006); Orphal and Ruth (2008); Vaughan et al. (2008); Washenfelder et al. (2008); Langridge et al. (2008); Varma et al. (2009); Chen and Venables (2011); Chen et al. (2011); Kahan et al. (2012) applied the Broad Band (BB) CEAS using broad band light sources. Ball et al. (2004) combined

AMTD
5, 3079–3115, 2012

BBCEAS for the data evaluation with the established DOAS technique (Platt and Stutz, 2008), creating the CE-DOAS. With this technique different trace gases could be detected simultaneously and at high spatial resolution (Ball et al., 2004; Gherman et al., 2008; Platt et al., 2009; Meinen et al., 2010; Thalman and Volkamer, 2010). We note that the BBCEAS retrieval algorithm from Fiedler et al. (2003) relies -like DOAS- on the characteristic narrow band absorption features of the molecules for their quantification and is thus in principle also a DOAS approach. The theoretical description of CE-DOAS can be found in Platt et al. (2009).

This paper describes the design and development of a specific CE-DOAS instrument, which for the first time identifies BrO in the UV-wavelength range (325–365 nm) by applying a UV-LED. To estimate the optical path length in the cavity, the instrument applies the CRD-technique (Meinen et al., 2010) and additionally the measurements of the trace gases O_4, O_3, and HONO. At the Atmospheric Chemistry Research Laboratory, University of Bayreuth, Germany first laboratory tests were successfully performed and the detection limits for different trace gases were determined.

2 Method: Cavity-Enhanced Differential Absorption Spectroscopy (CE-DOAS)

The basic idea of the CE-DOAS technique is to introduce incoherent broadband radiation I_L into an optical resonator (see Fig. 1), consisting of two mirrors with reflectivity R (for simplicity we assume both mirrors to have the same reflectivity, if the mirrors have different reflectivities R_1, R_2 an averaged reflectivity $R = \sqrt{R_1 R_2}$ is used). The distance between the mirrors is d_0 (see Fig. 1). Initially only the fraction $\rho = 1 - R$ of the radiation I_L enters the resonator. Here for simplicity I_L means only the fraction of the radiation from the LED which can be imaged into the resonator. (It is obvious that not all radiation emitted by the LED is going through the lens and also passes the aperture defined by mirror M_2.) Once inside the resonator, the radiation is reflected on average about $1/(1-R)$ times (neglecting other losses). Finally, in the absence of any extinction in the resonator, half of the radiation leaves the resonator through each mirror. Each

AMTD
5, 3079–3115, 2012

fraction has the intensity I_0. An effective mirror reflectivity $R_0(\lambda)$ is defined to include the Rayleigh extinction coefficient $\epsilon_R(\lambda)$ of pure air:

$$R_0(\lambda) = R(\lambda) - \epsilon_R(\lambda) d_0 \quad (1)$$

or

$$\rho_0(\lambda) = 1 - R_0(\lambda) = 1 - R(\lambda) + \epsilon_R(\lambda) d_0 = \rho(\lambda) + \epsilon_R(\lambda) d_0 \quad (2)$$

In this paper the index 0 always corresponds to the cavity without absorbers but including Rayleigh scattering.

2.1 Continuous data collection

DOAS techniques derive the trace gas concentration by the use of the optical density $D(\lambda)$ which requires the measurement of the intensities without ($I_0(\lambda)$) and with ($I(\lambda)$) trace gas absorption (Platt and Stutz, 2008). In a CE-DOAS setup the optical density D_{CE} is determined from intensity measurements with absorber free filled (e.g. synthetic air) resonator I_{tot0} and with sample air filled resonator I_{tot}:

$$D_{CE} = \ln\left(\frac{I_{tot0}}{I_{tot}}\right) = \ln\left(\frac{\int_0^\infty I_{in0}(n)\mathrm{d}n}{\int_0^\infty I_{in}(n)\mathrm{d}n}\right) = \ln\left(1 + \frac{\tau}{\rho_0}\right) \quad (3)$$

$I_{in0}(n)$ is the intensity after n passes through the cavity in the pure air filled cavity (without any absorbers) and $I_{in}(n)$ is the intensity after n passes through the cavity including also absorptions. n is the number of traverses of the photons through the cavity. τ = 1-transmissivity of the cavity. However according to Platt et al. (2009) for strong absorptions this is not equal to the optical density used in traditional DOAS application if using the average light path from Sect. 2.2. Thus the corrections from Sect. 2.4 have to be applied.

AMTD
5, 3079–3115, 2012

2.2 Determination of the average light path

According to Platt et al. (2009) the average length of the light path $\bar{L}(\lambda)$ is expressed by:

$$\bar{L}(\lambda) \approx \frac{d_0}{\tau(\lambda) + \rho(\lambda)} = \frac{d_0}{\sigma(\lambda)\bar{c}d_0 + \rho_0(\lambda)} \quad (4)$$

$\sigma(\lambda)$ is the absorption cross section of the trace gas and $\bar{c}$ the average trace gas concentration in the cavity. Note that the transmission of the cavity, $\tau(\lambda)$ includes all extinction processes in the cavity i.e. aerosol absorption and Mie scattering as well as absorption by trace gases. It does not include extinction by pure air due to absorption and Rayleigh scattering. This is taken into account by using $\rho_0(\lambda)$ instead of $\rho(\lambda)$. For an air filled resonator that results in:

$$\bar{L}_0(\lambda) = \frac{d_0}{\rho_0(\lambda)} \quad (5)$$

In praxis this average path length $\bar{L}_0(\lambda)$ can be determined e.g. from the known Rayleigh scattering of two different gases for example He and dry zero air (Washenfelder et al., 2008), from a CRD decay time measurement (Meinen et al., 2010), or from the differential absorption of a trace gas of known concentration. In this work $\bar{L}_0(\lambda)$ was determined from the absorption bands of O_4 at 343.5 nm and 360.4 nm making use of the known O_2 concentration (Ball et al., 2004). How this average path length has to be corrected yet, is described in the following subsections.

2.3 Correction of the base path-length

The length of the absorption medium in the resonator d is not necessarily equal to the distance between the mirrors d_0 (see Fig. 2), since at either end of the resonator a few centimeters of the path are not filled with air due to a purge flow close to the mirrors. In

AMTD
5, 3079–3115, 2012

this case the effective light path has to be corrected by the factor d/d_0.

$$\bar{L}(\lambda) = \bar{L}_0(\lambda)\frac{d}{d_0} \tag{6}$$

2.4 Correction for light path reduction due to extinction in the cavity

Platt et al. (2009) describe in detail how the light path is reduced by extinction in the resonator. Here two out of the four ways to correct this effect presented by Platt et al. (2009) are applied. For both ways the optical density D_{CE} and the average path length $\bar{L}(\lambda)$ needs to be known.

1. Correction of the trace gas absorption cross section σ to σ_{eff}:

$$\sigma_{eff}(\lambda) = \sigma(\lambda) \times \frac{\bar{L}_{eff}(\lambda)}{\bar{L}(\lambda)} = \sigma(\lambda) \times \frac{D_{CE}}{e^{D_{CE}} - 1} \tag{7}$$

   This σ_{eff} is used by a DOAS-fit to obtain a corrected column density. From this column density the corrected concentration is determined by dividing with $\bar{L}(\lambda)$. This method is used iteratively for measurements with only one trace gas and without aerosols where the convoluted reference cross section σ_0 is corrected. During the first iteration a DOAS fit determines an optical density D_0 and σ_0 is corrected to σ_1. In the next iteration step σ_1 determines a D_1 and σ_0 is corrected to σ_2, etc:

   i. iteration:

$$\sigma_i \rightarrow (cL)_i \rightarrow (cL)_i \times \sigma_i = D_i \rightarrow \sigma_0 \times \frac{D_i}{e^{D_i} - 1} = \sigma_{i+1} \tag{8}$$

   We applied this correction in four iteration steps. The same method can also be applied if several absorbers are present by extending Eq. (8).

AMTD
5, 3079–3115, 2012

2. Method 1 with Eq. (7) becomes very complex when using more than one absorber. In this case a second method is useful in order to correct the optical density before the fit and convert it to D_{eff} which is equal to an absorption where the light path is not reduced:

$$D_{\mathrm{eff}} = e^{D_{\mathrm{CE}}} - 1 = \frac{I_{0\mathrm{tot}}}{I_{\mathrm{tot}}} - 1 \tag{9}$$

In this work the second method applying Eq. (9) is used whenever there is more than one absorber. It needs to be considered that for this correction the intensities $I_{0\mathrm{tot}}$ and I_{tot} have to be successively measured. This requires an absolutely stable optical resonator and light source intensity (similar to the requirements of the BBCEAS approach).

2.5 Correction of the wavelength dependence of the average light path

As described in Sect. 2.2 the average light path $\bar{L}(\lambda)$ is dependent on λ because $R(\lambda)$ is dependent on λ. As described by Venables et al. (2006) it is possible to use differential absorption structures for the determination of the wavelength dependence of the mirror reflectivity and therefore for the calibration of the path length. This method requires an absorber of known concentration, which has several distinct absorption bands in the wavelength range of interest. In the present study, we used O_3 and HONO to estimate the relative shape of the reflection curve. Since the concentration of these gases was unknown the absorption bands of O_4 at 343.5 nm and 360.4 nm were used additionally to derive the absolute reflectivity curve of the mirrors.

3 Experimental

3.1 The instrument

Figure 1 shows a schematic diagram of the CE-DOAS instrument (more details can be found at Hoch (2010). The radiation of a pulsed UV-LED is imaged by lens L_1

AMTD
5, 3079–3115, 2012

into the resonator, consisting of two high reflective dielectric mirrors m_1 and m_2 (focal length = 1 m). The radiation, which leaves the resonator through m_2, is focused by the lens L_2 into a fiber bundle which can be adjusted by a x-y stage. This fiber bundle transmits the light to a temperature-stabilized spectrograph (Ocean Optics QE 65000). The movable mirror "K" can redirect the light to a photomultiplier (PMT) to record a ring-down signal and thus check the quality of the resonator. F_1 and F_2 are band-pass filters. F_1 protects the PMT and F_2 shields the fibers from scattered light and LED light beneath of the reflectivity range of the mirrors. The shutter is used to perform background measurements without radiation of the UV-LED. The electronic controller receives a constant current and creates the pulses for the UV-LED. It also controls the shutter and the mirror "K".

3.1.1 The LED radiation source

The wavelength range (325 nm to 365 nm) of the LED UVTOP340 from Sensor Electronic Technology was chosen to optimize the sensitivity to BrO while minimizing the interference due to O_3. To minimize the known LEDs etalon structures the LED is inclined against the optical axis of the resonator at an angle of 15° (Sihler et al., 2009). For CRD-measurements the LED has to be operated in a pulsed mode. Extensive noise characterizations of the LED showed that permanent pulsing of the LED creates less spectral noise than a periodic change between pulsing and continous operation. Therefore the LED is permanently pulsed with 750 µs (on) and 50 µs (off) also for recording spectra with the spectrometer.

3.1.2 Mirrors and optics

The core of the setup is the resonator which consists of two high reflective mirrors (Fig. 1, m_1 and m_2). The reflectivity of the mirrors from LAYERTEC GmbH, (Mellingen, Germany) was chosen to achieve a good compromise between optical light path length and signal to noise ratio (Fiedler et al., 2007). The radiation of the UV-LED is

AMTD
5, 3079–3115, 2012

coupled into the resonator by lens L_1 ($F_1 = 25$ mm) to use as much of the LED output as possible. The radiation which passes mirror m_2 is focused by lens L_2 ($F_2 = 100$ mm) on a fiber coupler to match the numerical aperture (NA[1]) of the spectrometer. The fiber bundle (Loptek GmbH & Co, Berlin, Germany) consists of seven 200 µm fibers (NA of 0.22, UV solarization stabilized, 6 m long), arranged in a circular configuration on the resonators side and column configuration at the spectrometers side. The band-pass filter F_1 and F_2, both UG11 from Schott, (Mainz, Germany) have a transmission range of 270–380 nm and a thickness of 1 mm. F_1 was placed directly in front of the PMT protect the device as much as possible against ambient light (e.g. if cover is opened). The reflectivity of the mirrors can not readily be derived from the manufacturer's data: Layertec provided transmission values (T) but not reflectivities. Since $R + T + A = 1$ (A = Absorption) R can not be calculated from T unless the absorption A in the dielectric mirror is negligible, which, unfortunately, is not the case in this wavelength range. We used two sets of mirrors with different values of stated transmissivity at 340 nm: M_1: $T = 0.048$ %, M_2: $T = 0.11$ %.

3.1.3 Spectrograph and detector

The fiber transmits the light into a temperature stabilized (20 °C) spectrograph QE65000 from Ocean Optics (Dunedin, Florida, USA). The spectrometer has a focal length of 101 mm, it is equipped with a 2400 lines/mm grating resulting in 0.62 nm spectral resolution with the column of seven 200 µm fibers (see Subsect. 3.1.2) acting as entrance slit.

The detector used in the QE65000 spectrometer is a scientific-grade, back-thinned, Thermo-Electrically Cooled (TEC), 1044 × 64 element CCD array (S7031-1006 from Hamamatsu Photonics (Naka-ku, Hamamatsu City, Shizuoka Pref., Japan)), temperature stabilized to −20 °C.

[1] NA = $n \sin(\alpha/2)$, n = index of refraction = 1.0(air), α = angular aperture (maximum cone of light that can enter or exit the optical device of interest)

AMTD
5, 3079–3115, 2012

3.1.4 Photomultiplier (PMT) for CRD

For the ring down measurement the radiation intensity is measured by a PMT (H578-01 from Hamamatsu Photonics (Naka-ku, Hamamatsu City, Shizuoka Pref., Japan)). As current amplifier a DLPCA-100 from FEMTO Messtechnik GmbH, (Berlin, Germany) is applied. A PC-oscilloscope DAQSCOPE PCI-5102 from National Instruments (Austin, Texas, USA) records the ring down signal.

3.1.5 Software

The program DOASIS (Kraus, 2004) is used to carry out and analyze the spectra.

To acquire the CRD signals a dedicated program was developed with LabVIEW from National Instruments. This program receive the ring down signal from the PC-oscilloscope, calculates the mean of a given number of measurements and fits a double exponential decay $f(t)$ (Eq. 10).

$$f(t) = A \times \left(\frac{\tau_1}{\tau_1 - \tau_2} \times e^{-\frac{t}{\tau_1}} - \frac{\tau_2}{\tau_1 - \tau_2} \times e^{-\frac{t}{\tau_2}} \right) + b \tag{10}$$

τ_1 denotes the electro-optical decay time from electronics and LED and τ_2 for the CRD-decay time. Also A denotes the initial signal at $t = 0$ and b denotes any offset signal at $t = \infty$. From this fit and known τ_1 the CRD-decay time can be determined and converted to a optical light path or mirrors reflectivity according to Meinen et al. (2010). However in our case it is not possible to derive with this method the accurate absorption light path for the data evaluation, as the mirror reflectivity varies too much over the LED spectral range (see Sect. 2.5). Nevertheless, τ_2 just gives an indication of the wavelength averaged light path, which is used to monitor the contamination of the mirrors and allow quick action to optimize instrument performance.

AMTD
5, 3079–3115, 2012

3.2 The measurement setup

The instrument was developed and characterized at the Institute for Environmental Physics (IUP) in Heidelberg, Germany. After first successful measurements, it was applied for the observation of different trace gases at the Atmospheric Chemistry Research Laboratory, University of Bayreuth, Germany. For these measurements the instrument was used as it is described in Sect. 3.1 and shown in Fig. 1. Two hermetically sealed plastic boxes were placed around the optical component assemblies in order to protect the sensitive optics against dust and other extreme conditions for planned measurements in a climate chamber. Furthermore the hermetically sealed containment guarantee a stable nitrogen purge-flow (1 l min^{-1}) of the resonator mirrors to prevent them from contaminations from the measurement air. Otherwise the overpressure in the chamber may cause an airflow beside the mirrors and thus cause contaminations. For the measurements described in the following an air tight chamber was placed between the two boxes containing the mirrors and associated optics (Fig. 2). This chamber could be filled through three gas inlets/outlets with different gases. Three different set-ups with various base-path lengths were used: one with a glass chamber (setup A) and two with Teflon chambers (setup B and C). Table 1 shows the sizes of these three chambers and Table 2 gives an overview of the different trace gas measurement setups. With these setups, different trace gas measurements were carried out: O_3 and HONO were measured mainly in order to determine the wavelength dependency of the reflectivity and the optical path length, O_4 measurements were performed in order to determine the absolute optical path length at two particular wavelengths (343.4 nm and 360.5 nm) and BrO and HCHO measurements to determine their detection limits. Before each trace gas measurement, offset (20 000 scans and 8 ms integration time) and dark current (1 scan and 30 000 ms integration time) spectra were taken with blocked LED. In the next step a CRD measurement with 1000 average determinations was performed to determine possible mirror contamination. A spectrum with 85 % of full saturation could be obtained in 9.50 s with mirror set M_1 and 3.50 s with mirror set

AMTD
5, 3079–3115, 2012

M_2. Based on noise tests, 30 spectral scans were taken and co-added for mirror set M_1 and 50 spectral scans were taken and co-added for mirror set M_2 to achieve sufficient measurement accuracy. This corresponds to a temporal resolution of 4.8 min for M_1 and 2.9 min for M_2. The measurements shown within this study were undertaken without the presence of aerosols.

3.2.1 Ozone measurements

For the O_3 measurements the setups B and C with Teflon chamber were used. For setup B mirror set M_2 and for setup C mirror set M_1 was used (Table 2). To determine an I_0 spectrum the chamber was filled with nitrogen and the mirrors were purge with nitrogen, too. Afterwards O_3 was produced and filled into the chamber through the gas inlet. The gas outlets were connected to an active charcoal trap. In setup B the ozone was created by ionization of O_2 (purity = 99.995 %) using a corona discharge ozonizer and in setup C by passing O_2 (purity = 99.995 %) along four pen-ray mercury discharge lamps.

3.2.2 Nitrous acid measurements

For the nitrous acid (HONO) measurements setup B with mirror set M_2 and setup C with mirror set M_1 was used (see Table 2), similar to the setup for O_3 measurements. The generation of the nitrous acid is based on the reaction of a sodium nitrite solution $NaNO_2$ with sulfuric acid H_2SO_4 as e.g. described by Taira and Kanda (1990):

$$H_2SO_4 + NaNO_2 \rightarrow NaHSO_4 + HONO \quad \text{(R1)}$$

The reaction takes place in a glass vessel with a glass frit at its base. The diluted solutions of sodium nitrite and sulfuric acid are continuously pumped into a reaction vessel and the mixture is then drawn off to waste. A carrier gas, here nitrogen, is introduced into the reagent mixture through the frit and continuously purges nitrous acid vapor from the mixture. The HONO generation depends on temperature, gas flow, $NaNO_2$ concentration and fluid flow. A typical concentration up to 30 ppb was accomplished.

AMTD
5, 3079–3115, 2012

3.2.3 Oxygen dimer measurements

In order to determine the light path in the cavity at two particular wavelengths (343.4 nm and 360.5 nm), O_4 measurements were carried out. For that purpose the resonator was first completely filled with nitrogen and afterwards completely (including mirror purge gas) with pure oxygen. Additionally barometric pressure (with a mercury barometer) and temperature were measured to determine the O_2 concentration in the resonator. With the absorption of O_4 at 343.4 nm and 360.5 nm the light path at these wavelengths could be determined.

3.2.4 Bromine monoxide measurements

BrO measurements were carried out in setup B with mirror set M_2 and in setup C with mirror set M_1 (see Table 2). For these measurements the mirror protection tubes were purged with nitrogen. The gas outlets are connected to a pump producing a slight underpressure. First O_3 was admitted through the gas inlet and afterwards Br_2. A fluorescent tube (Philips TL/12, 40W, UV A and UV B) set up next (at 20 cm distance) to the chamber was switched on to photolyze Br_2. Evaluation and results of these measurements are described in Sect. 4.

4 Data evaluation and results

The software DOASIS (Kraus, 2004) was used for the analysis of the recorded spectra as described in Sect. 3.1. The wavelength calibration of the spectrometer/detector was done with the help of the line spectra of a mercury lamp. For convolution of the literature absorption cross sections (overview in Table 3) with the instrument function the recorded line shape at 334.14 nm of this lamp was used.

AMTD
5, 3079–3115, 2012

4.1 Mirror reflectivity and path length calibration

As described in Sect. 2.5 it is possible to use differential absorption structures to derive the wavelength dependence of the mirror reflectivity and therefore for the determination of the wavelength dependent path length.

We used O_3 and HONO to estimate the relative shape of the mirror reflectivity, not the absolute, as the actual concentrations were unknown. The used fit windows are shown in Table 4. With the additional absorption bands of O_4 at 343.4 nm and 360.5 nm, the absolute reflectivity curve of the mirrors could be determined with known concentration of O_4. The absolute reflectivity curves are shown in Fig. 3. The following measurements were corrected with those reflectivity curves. The absorption A of the mirrors can be derived from the data in Fig. 3 as:

$$A = (1 - T) - R \tag{11}$$

The absorptions of both mirror sets are of the order of $A = 4 \times 10^{-4}$. According to Fiedler et al. (2007) the relation between optical light path length and signal to noise ratio Q can be determined with:

$$Q = \frac{(1 - R - A)[1 + (1 - L)^2 R^2]}{\sqrt{[1 - (1 - L)^2 R^2]^3}} \tag{12}$$

Figure 4 shows the enhancement factor (quality factor) Q dependency on $(1 - R)$ assuming $A = 4 \times 10^{-4}$. Based on this theory, we expected a lower detection limit for a reflectivity of $R_2 = 0.9984$ of M_2 than for M_1 ($R_1 = 0.9991$), if the measurement accuracy is purely dominated by photon noise.

4.2 Detection limits

The true 1σ error of the measurement for the different trace gases are obtained from the statistical 1σ error of the DOAS fit, by multiplying with a factor of 2.5, as the fit error

AMTD
5, 3079–3115, 2012

underestimates the true measurement error (Stutz and Platt, 1996). For the estimation of this error, the number of absorption bands, the number of channels used for evaluation, the intensity of the recorded spectrum, uncertainties in the wavelength-pixel mapping and the scale and structures in the residual spectrum are taken into account. The values are derived for measurements with relative high trace gas concentrations. Thus measurement error and detection limit may be lower for lower concentrations due to less structures in the residual spectrum. The detection limit is given as twice the 1σ measurement error. In Figs. 5, 6, 7, and 8 example fits of different trace gases are shown. In Table 5 the detection limits for the measured trace gases for the two different mirror sets and different integration times are given. Based on the theory of Fiedler et al. (2007) we expected a better detection limit for the lower reflectivity of $R_2 = 0.9984$ of M_2 than for M_1 ($R_1 = 0.9991$). However we observed a better detection limit for M_1 compared to M_2. The reason is that the detection limit of a DOAS-measurement is not only dependent on the photon noise, but also on spectral structures, which are not constant in time. Other sources for increasing noise are electronic noise and optical noise e.g. introduced by the LED light source, optical fibers and spatial inhomogeneity of the optical grating of the spectrograph.

5 Conclusions

We developed the first LED based CE-DOAS detection of BrO in the UV-wavelength-range from 325 nm to 365 nm and achieved a detection limit of 11 ppt using a time resolution of 81 min per measurement. Besides BrO also HONO, HCHO, O_3 as well as O_4 were detected in this wavelength-range. The detection limits were 450 ppt for HONO, 5.1 ppb for HCHO, and 59 ppb for O_3. These figures are quite adequate for simulation-chamber measurements, where e.g. BrO levels up to 6000 ppt were observed (Buxmann et al., 2012).

The relative dependence of the mirror reflectivity and thus path length on the wavelength was derived using the absorption structures of O_3 and HONO. With an O_4

AMTD
5, 3079–3115, 2012

measurement at a known O_2 concentration we calculated the absolute optical path length at the absorption band. Combining these data with the relative path length the absolute wavelength dependent mirror reflectivity and path length of the whole wavelength-range was derived. We used two sets of mirrors with different maximal reflectivity values at 347 nm for M_1 of $R_1 = 0.9991$ (transmission = 0.05 %) and for M_2 of $R_2 = 0.9984$ (transmission = 0.12 %). We determined the absorption for both mirror sets to be in the range of 4×10^{-4} at 347 nm. The absorption is increasing towards smaller wavelengths, so that the peak of the reflectivity is shifted towards larger wavelength compared to the transmission of the mirrors.

In contrast to expectation from the theory of Fiedler et al. (2007) we found a better detection limit for the higher reflectivity of $R_1 = 0.9991$ of M_1 than for M_2 ($R_2 = 0.9984$). The reason is that the detection limit of a DOAS-measurement is not only dependent on the photon noise, but also of spectral structures which are not constant in time. Other sources for increasing noise are electronic noise and optical noise like the LED light source, optical fibers and spatial inhomogeneity of the optical grating of the spectrograph.

Several options are available for improvement of the system in the future: mirrors with higher reflectivity can be an improvement, if the absorption of the mirrors can be reduced (e.g. by using different materials during the production process). With the current absorptions, a higher reflectivity will not give an improvement. The base path length could also be expanded, but at the expense of compactness and ease of handling of the instrument set up.

Another aim is to increase the light intensity for a better time resolution and therefore improved detection limit. The intensity of UV-LEDs is still very poor, but its improvement is a topic of current research. Cooling of the LED looks also promising, since cooling of 30 K down to −10 °C was found to increase the radiation intensity up to 46 %. Further cooling did not have any effect, although it could be expected from the data sheet (SET, 2010).

AMTD
5, 3079–3115, 2012

The system could be improved with a spectrometer with higher light throughput and larger entrance slit area to use more of the radiating exiting the cavity.

For validation of the achieved measurements we plan a comparison campaign with an active DOAS instrument in combination with a well established multi-reflection cell (White, 1976; Ritz et al., 1993; Volkamer et al., 2002; Hak et al., 2005; Buxmann et al., 2012; Ofner et al., 2012) at Bayreuth.

Due to its compact size and low power consumption it is possible to apply the BrO CE-DOAS-instrument -besides in reaction chamber investigations- also for field studies with batteries even if other electrical power is not available. There are several areas where BrO has been detected in the atmosphere at levels exceeding the detection limit of our CE-DOAS instrument, e.g. in arctic regions 41 ppt (Pöhler et al., 2010), at the Salar de Uyuni, Bolivia up to 20 ppt (Hönninger et al., 2004), at the Dead Sea 200 ppt (Hebestreit et al., 1999; Matveev et al., 2001; Tas et al., 2008), or in volcanic plumes, where BrO mixing ratios of the order of 1000 ppt were inferred (Bobrowski et al., 2003). All these observations are averaged concentrations over few km long light paths. Thus the BrO CE-DOAS instrument can help to study the involved processes by deriving in-situ BrO concentrations.

Acknowledgements. We are grateful to the German Science Foundation (DFG) for funding the research unit 763, HALOPROC, to H.-U. Krüger[2] for technical support, to M. Sörgel for generation of HONO and to J. Ofner, S. Bleicher, and N. Balzer for helping with the chemical tasks.

References

Ball, S. M. and Jones, R. L.: Broad-Band Cavity Ring-Down Spectroscopy, Chem. Rev., 103, 5239–5262, 2003. 3081

Ball, S. M., Povey, I. M., Norton, E. G., and Jones, R. L.: Broadband cavity ringdown spectroscopy of the NO_3 radical, Chem. Phys. Lett., 342, 113–120, 2001. 3081

[2]deceased

AMTD
5, 3079–3115, 2012

Ball, S. M., Langridge, J., and Jones, R.: Broadband cavity enhanced absorption spectroscopy using light emitting diodes, Chem. Phys. Lett., 398, 68–74, 2004. 3081, 3082, 3084
Barrie, L. A., Bottenheim, J., Schnell, R., Crutzen, P., and Rasmussen, R.: Ozone destruction and photochemical reactions at polar sunrise in the lower Arctic atmosphere, Nature, 334, 138–141, 1988. 3080
Barrie, L. A., Bottenheim, J. W., and Hart, W. R.: Polar Sunrise Experiment 1992 (PSE 1992): Preface, J. Geophys. Res., 99, 25313–25314, 1994. 3080
Bobrowski, N., Hönninger, G., Galle, B., and Platt, U.: Detection of Bromine Monoxide in a Volcanic Plume, Nature, 423, 273–276, 2003. 3096
Bottenheim, J. W., Gallant, A. C., and Brice, K.: Measurements of NO_y species and O_3 at 82° N latitude, Geophys. Res. Lett., 13, 113–116, 1986. 3080
Bottenheim, J. W., Barrie, L. A., Atlas, E., Heidt, L. E., Niki, H., Rasmussen, R. A., and Shepson, P. B.: Depletion of lower tropospheric ozone during Arctic spring: The polar sunrise experiment 1988, J. Geophys. Res., 95, 18555–18568, 1990. 3080
Buxmann, J., Balzer, N., Bleicher, S., Platt, U., and Zetzsch, K.: Observations of bromine explosions in smog chamber experiments above a model salt pan, Int. J. Chem. Kinet., in press, 2012. 3094, 3096
Chen, J. and Venables, D. S.: A broadband optical cavity spectrometer for measuring weak near-ultraviolet absorption spectra of gases, Atmos. Meas. Tech., 4, 425–436, doi:10.5194/amt-4-425-2011, 2011. 3081
Chen, J., Wenger, J., and Venables., D.: Near-ultraviolet absorption cross sections of nitrophenols and their potential influence on tropospheric oxidation capacity, J. Phys. Chem. A, 115, 12235–12242, doi:10.1021/jp206929r, 2011. 3081
Engeln, R., Berden, G., Peeters, R., and Meijer, G.: Cavity enhanced absorption and cavity enhanced magnetic rotation spectroscopy, Rev. Sci. Instrum., 69, 3763–3769, 1998. 3081
Fawcett, B. L., Parkes, A. M., Shallcross, D. E., and Orr-Ewing, A. J.: Trace detection of methane using continuous wave cavity ring-down spectroscopy at 1.65 µm, Phys. Chem. Chem. Phys., 4, 5960–5965, 2002. 3081
Fiedler, S., Hese, A., and Ruth, A. A.: Incoherent broad-band cavity-enhanced absorption spectroscopy, Chem. Phys. Lett., 371, 284–294, doi:10.1016/S0009-2614(03)00263-X, 2003. 3081, 3082

AMTD
5, 3079–3115, 2012

Fiedler, S., Hese, A., and Heitmann, U.: Influence of the cavity parameters on the output intensity in incoherent broadband cavity-enhanced absorption spectroscopy, Rev. Sci. Instrum., 78, 073104, doi:10.1063/1.2752608, 2007. 3087, 3093, 3094, 3095, 3111

Fleischmann, O. C. and Burrows, J.: New ultraviolet absorption cross-sections of BrO at atmospheric temperatures measured by time-windowing fourier transform spectroscopy, J. Photochem. Photobiol. A: Chem., 168, 117–132, 2004. 3105

Friess, U., Sihler, H., Sander, R., Poehler, D., Yilmaz, S., and Platt, U.: The vertical distribution of BrO and aerosols in the Arctic: Measurements by active and passive differential optical absorption spectroscopy, J. Geophys. Res.-Atmos., 116, D00R04, doi:10.1029/2011JD015938, 2011. 3081

Gherman, T., Venables, D. S., Vaughan, S., Orphal, J., and Ruth, A. A.: Incoherent broadband cavity-enhanced absorption spectroscopy in the near-ultraviolet: application to HONO and NO_2, Environ. Sci. Technol., 42, 820–895, 2008. 3082

Greenblatt, G. D., Orlando, J. J., Burkholder, J. B., and Ravishankara, A. R.: Absorption measurements of oxygen between 330 and 1140 nm, J. Geophys. Res.-Atmos., 95, 18577–18582, 1990. 3105

Hak, C., Pundt, I., Trick, S., Kern, C., Platt, U., Dommen, J., Ordóñez, C., Prévôt, A. S. H., Junkermann, W., Astorga-Lloréns, C., Larsen, B. R., Mellqvist, J., Strandberg, A., Yu, Y., Galle, B., Kleffmann, J., Lörzer, J. C., Braathen, G. O., and Volkamer, R.: Intercomparison of four different in-situ techniques for ambient formaldehyde measurements in urban air, Atmos. Chem. Phys., 5, 2881–2900, doi:10.5194/acp-5-2881-2005, 2005. 3096

Hebestreit, K., Stutz, J., Rosen, D., Matveiv, V., Peleg, M., Luria, M., and Platt, U.: DOAS measurements of tropospheric bromine oxide in mid-latitudes, Science, 283, 55–57, 1999. 3081, 3096

Hönninger, G., Bobrowski, N., Palenque, E., Torrez, R., and Platt, U.: Reactive bromine and sulfur emissions at Salar de Uyuni, Bolivia, Geophys. Res. Lett., 31, L04101, doi:10.1029/2003GL018818, 2004. 3081, 3096

Hoch, D. J.: Resonator Verstärkte Differentielle Optische Absorptions Spektroskopie: Labormessungen von BrO, HCHO, HONO und O_3, Master's thesis, Inst. for Environmental Physics (IUP), Atmosphere and Remote Sensing, Ruprecht-Karls-Universität Heidelberg, Germany, 2010. 3086

AMTD
5, 3079–3115, 2012

Kahan, T. F., Washenfelder, R. A., Vaida, V., and Brown, S. S.: Cavity-enhanced measurements of hydrogen peroxide absorption cross sections from 353 to 410 nm, J. Phys. Chem. A, in press, doi:10.1021/jp2104616, 2012. 3081

Kraus, S.: DOASIS: DOAS Intelligent Sytem, Software, copyright 2004 Stefan Kraus, Institute of Environmental Physics, University of Heidleberg, Germany, in cooperation with Hoffmann Messtechnik GmbH, 2004. 3089, 3092

Kreher, K., Johnston, P. V., Wood, S. W., and Platt, U.: Ground-based measurements of tropospheric and stratospheric BrO at Arrival Heights, Antarctica, Geophys. Res. Lett., 24, 3021–3024, doi:10.1029/97GL02997, 1997. 3080

Langridge, J. M., Ball, S. M., and Jones, R. L.: A compact broadband cavity enhanced absorption spectrometer for detection of atmospheric NO_2 using light emitting diodes, Analyst, 131, 916–922, 2006. 3081

Langridge, J. M., Laurila, T., Watt, R. S., Jones, R. L., Kaminski, C. F., and Hult, J.: Cavity enhanced absorption spectroscopy of multiple trace gas species using a supercontinuum radiation source, Opt. Express, 16, 10178–10188, 2008. 3081

Leser, H., Hönninger, G., and Platt, U.: MAX-DOAS measurements of BrO and NO_2 in the marine boundary layer, Geophys. Res. Lett., 30, 1537, doi:10.1029/2002GL015811, 2003. 3081

Mahajan, A. S., Plane, J. M. C., Oetjen, H., Mendes, L., Saunders, R. W., Saiz-Lopez, A., Jones, C. E., Carpenter, L. J., and McFiggans, G. B.: Measurement and modelling of tropospheric reactive halogen species over the tropical Atlantic Ocean, Atmos. Chem. Phys., 10, 4611–4624, doi:10.5194/acp-10-4611-2010, 2010. 3081

Matveev, V., Peleg, M., Rosen, D., Tov-Alper, D. S., Hebestreit, K., Stutz, J., Platt, U., Blake, D., and Luria, M.: Bromine oxide – ozone interaction over the Dead Sea, J. Geophys. Res., 106, 10375–10387, 2001. 3081, 3096

Meinen, J., Thieser, J., Platt, U., and Leisner, T.: Technical Note: Using a high finesse optical resonator to provide a long light path for differential optical absorption spectroscopy: CE-DOAS, Atmos. Chem. Phys., 10, 3901–3914, doi:10.5194/acp-10-3901-2010, 2010. 3082, 3084, 3089

Meller, R. and Moortgat, G.: Temperature dependence of the absorption cross sections of formaldehyde between 223 and 323 K in the wavelength range 225–375 nm, J. Geophys. Res.-Atmos., 105, 7089–7101, 2000. 3105

AMTD
5, 3079–3115, 2012

Ofner, J., Balzer, N., Buxmann, J., Grothe, H., Schmitt-Kopplin, P., Platt, U., and Zetzsch, C.: Halogenation processes of secondary organic aerosol and implications on halogen release mechanisms, Atmos. Chem. Phys. Discuss., 12, 2975–3017, doi:10.5194/acpd-12-2975-2012, 2012. 3096

O'Keefe, A. and Deacon, D.: Cavity ring-down optical spectrometer for absorption measurements using pulsed laser sources, Rev. Sci. Instrum., 59, 2544–2551, doi:10.1063/1.1139895, 1988. 3081

Orphal, J. and Ruth, A. A.: High-resolution Fourier-transform cavity-enhanced absorption spectroscopy in the near-infrared using an incoherent broad-band light source, Opt. Express, 16, 19232–19243, 2008. 3081

Paldus, B. A., Harb, C. C., Spence, T. G., Zare, R. N., Gmachl, C., Capasso, F., Sivco, D. L., Baillargeon, J. N., Hutchinson, A. L., and Cho, A. Y.: Cavity ringdown spectroscopy using mid-infrared quantum-cascade lasers, Opt. Express, 25, 666–668, 2000. 3081

Peeters, R., Berden, G., Apituley, A., and Meijer, G.: Open-path trace gas detection of ammonia based on cavity-enhanced absorption spectroscopy, Appl. Phys. B-Lasers O., 71, 231–236, 2000. 3081

Pöhler, D., Vogel, L., Friess, U., and Platt, U.: Observation of halogen species in the Amundsen Gulf, Arctic, by active long-path differential optical absorption spectroscopy, P. Natl. Acad. Sci. USA, 107, 6582–6587, 2010. 3081, 3096

Platt, U. and Lehrer, E.: Arctic Tropospheric Ozone Chemistry, ARCTOC, Final Report of the EU-Project No. EV5V-CT93-0318, Heidelberg, 1996. 3081

Platt, U. and Stutz, J.: Differential Optical Absorption Spectroscopy: Principles and Applications, Physics of Earth and Space Environments, Springer-Verlag Berlin Heidelberg, 2008. 3082, 3083

Platt, U., Meinen, J., Pöhler, D., and Leisner, T.: Broadband Cavity Enhanced Differential Optical Absorption Spectroscopy (CE-DOAS) – applicability and corrections, Atmos. Meas. Tech., 2, 713–723, doi:10.5194/amt-2-713-2009, 2009. 3082, 3083, 3084, 3085

Ritz, D., Hausmann, M., and Platt, U.: An improved open path multi-reflection cell for the measurement of NO_2 and NO_3, Optical Methods in Atmospheric Chemistry, edited by: Schiff, H. I. and Platt, U., 1715, 200–211, doi:10.1117/12.140211, 1993. 3096

Saiz-Lopez, A., Plane J. M. C, and Shillito J. A.: Bromine oxide in the mid-latitude marine boundary layer, Geophys. Res. Lett., 31, L03111, doi:10.1029/2003GL018956, 2004. 3081

Saiz-Lopez, A., Mahajan, A. S., Salmon, R. A., Bauguitte, S. J.-B., Jones, A. E., Roscoe, H. K., and Plane, J. M. C.: Boundary layer halogens in coastal Antarctica, Science, 317, 348–352, doi:10.1126/science.1141408, 2007. 3081

Schuster, G., Labazan, I., and Crowley, J. N.: A cavity ring down/cavity enhanced absorption device for measurement of ambient NO_3 and N_2O_5, Atmos. Meas. Tech., 2, 1–13, doi:10.5194/amt-2-1-2009, 2009. 3081

SET: UVTOP Technical Data, available at: http://www.s-et.com (last access: 23 April 2012), 2010. 3095

Sihler, H., Kern, C., Pöhler, D., and Platt, U.: Applying light-emitting diodes with narrowband emission features in differential spectroscopy, Opt. Lett., 34, 3716–3718, 2009. 3087

Simpson, W. R.: Continuous wave cavity ring-down spectroscopy applied to in situ detection of dinitrogen pentoxide (N_2O_5), Rev. Sci. Instrum., 74, 3442–3452, 2003. 3081

Sturges, W. T., Schnell, R. C., Landsberger, S., Oltmans, S. J., Harris, J. M., and Li, S.-M.: Chemical and meteorological influences on surface ozone destruction at Barrow, Alaska, during spring 1989, Atmos. Environ., 27A, 2851–2863, 1993. 3080

Stutz, J. and Platt, U.: Numerical analysis and estimation of the statistical error of differential optical absorption spectroscopy measurements with least-squares methods, Appl. Opt., 35, 6041–6053, doi:10.1364/AO.35.006041, 1996. 3094

Stutz, J., Kim, E., Platt, U., Bruno, P., Perrino, C., and Febo, A.: UV-visible absorption cross section of nitrous acid, J. Geophys. Res.-Atmos., 105, 14585–14592, 2000. 3105

Taira, M. and Kanda, Y.: Continuous generation system for low-concentration gaseous nitrous acid, Anal. Chem., 62, 630–633, doi:10.1021/ac00205a018, 1990. 3091

Tas, E., Peleg, M., Pedersen, D. U., Matveev, V., Biazar, A. P., and Luria, M.: Measurement-based modeling of bromine chemistry in the Dead Sea boundary layer – Part 2: The influence of NO_2 on bromine chemistry at mid-latitude areas, Atmos. Chem. Phys., 8, 4811–4821, doi:10.5194/acp-8-4811-2008, 2008. 3081, 3096

Thalman, R. and Volkamer, R.: Inherent calibration of a blue LED-CE-DOAS instrument to measure iodine oxide, glyoxal, methyl glyoxal, nitrogen dioxide, water vapour and aerosol extinction in open cavity mode, Atmos. Meas. Tech., 3, 1797–1814, doi:10.5194/amt-3-1797-2010, 2010. 3082

Varma, R. M., Venables, D. S., Ruth, A. A., Heitmann, U., Schlosser, E., and Dixneuf, S.: Long optical cavities for open-path monitoring of atmospheric trace gases and aerosol extinction, Appl. Opt., 48, B159–B171, 2009. 3081

AMTD
5, 3079–3115, 2012

Vaughan, S., Gherman, T., Ruth, A. A., and Orphal, J.: Incoherent broad-band cavity-enhanced absorption spectroscopy of the marine boundary layer species I-2, IO and OIO, Phys. Chem. Chem. Phys., 10, 4471–4477, 2008. 3081

Venables, D., Gherman, T., Orphal, J., Wenger, J., and Ruth, A.: High sensitivity in situ monitoring of NO_3 in an atmospheric simulation chamber using incoherent broadband cavity-enhanced absorption spectroscopy, Environ. Sci. Technol., 40, 6758–6763, 2006. 3081, 3086

Voigt, S., Orphal, J., Bogumil, K., and Burrows, J.: The temperature dependence (203–293 K) of the absorption cross sections of O_3 in the 230-850 nm region measured by Fourier-transform spectroscopy, J. Photochem. Photobiol. A: Chem., 143, 1–9, 2001. 3105

Voigt, S., Orphal, J., and Burrows, J.: The temperature and pressure dependence of the absorption cross-sections of NO_2 in the 250–800 nm region measured by Fourier-transform spectroscopy, J. Photochem. Photobiol. A: Chem., 149, 1–7, 2002. 3105

Volkamer, R., Junkermann, W., Wirtz, K., and Platt, U.: Formation of formaldehyde, glyoxal and methylglyoxal from the toluene + OH reaction in the presence of NO_x, poster presented at EGS XXVII General Assembly, Nice, France, 2002. 3096

Washenfelder, R. A., Langford, A. O., Fuchs, H., and Brown, S. S.: Measurement of glyoxal using an incoherent broadband cavity enhanced absorption spectrometer, Atmos. Chem. Phys., 8, 7779–7793, doi:10.5194/acp-8-7779-2008, 2008. 3081, 3084

White, J. U.: Very long optical paths in air, J. Opt. Soc. Am., 66, 411–416, 1976. 3096

Zalicki, P. and Zare, R.: Cavity ring-down spectroscopy for quantitative absorption measurements, J. Chem. Phys., 107, 2708–2717, 1995. 3081

AMTD
5, 3079–3115, 2012

Table 1. Overview of the chamber sizes and base-path lengths for set-ups A, B and C.

set-up (chamber type)	cavity length (d_0) [cm]	absorption length (d) [cm]
A (glass)	107 ± 1	47 ± 1
B (Teflon)	149 ± 1	127 ± 1
C (Teflon)	181 ± 1	159 ± 1

AMTD
5, 3079–3115, 2012

Table 2. Overview of the different trace gas measurement set-ups.

measurement	mirror set	set-up
O_3	M_1 and M_2	A
O_3	M_2	B
O_3	M_1	C
HONO	M_1 and M_2	A
HONO	M_2	B
HONO	M_1	C
BrO	M_2	B
BrO	M_1	C
O_4	M_1 and M_2	A
O_4	M_1	C

AMTD
5, 3079–3115, 2012

Table 3. Overview of the literature absorption cross sections used in the DOAS evaluation: for each trace gas a mean-spectral shift was determined from a measured spectrum with strong absorption. The cross sections were corrected with these mean shift (Pre-shift) and linked together for the following measurements. For all trace gases the following DOAS-fit settings were used: fit window 325–365 nm; high pass filter with 1000 iterations; 3rd degree polynomial; squeeze limited to ±2 % (of the total spectral range).

Trace gas	Reference	Pre-shift [nm]	Shift
BrO	Fleischmann and Burrows (2004)	0.153	free
HCHO	Meller and Moortgat (2000)	0.0018	linked to BrO
HONO	Stutz et al. (2000)	0.08221	linked to BrO
O_4	Greenblatt et al. (1990)	0.578	linked to BrO
O_3	Voigt et al. (2001)	0.206	linked to BrO
NO_2	Voigt et al. (2002)	0	linked to BrO

AMTD
5, 3079–3115, 2012

Table 4. DOAS-fit windows of O_3 and HONO for the determination of the relative wavelength dependent path length.

Fit window	for HONO [nm]	for O_3 [nm]
1	325.5–337.2	326.5–329.8
2	337.3–349.1	329.5–332.7
3	348.7–359.0	332.7–335.8
4	361.4–375.6	335.8–339.2
5		338.9–342.7
6		342.4–346.6

AMTD
5, 3079–3115, 2012

Table 5. Detection limits for different measurement configurations. Mirror set M_1 with $R_1 = 0.9991$ and M_2 with $R_2 = 0.9984$.

trace gas	mirrors	path length [m]	integration time [min]	det. lim. [ppt]	integration time [min]	det. lim. [ppt]
BrO	M_2	839	2.9	41	61.3	17
BrO	M_1	1472	4.8	20	80.8	11
HCHO	M_2	839	2.9	9100	61.3	5100
HONO	M_1	1472	4.8	970	106	450
O_3	M_1	1472	4.8	91 000	47.5	59 000

AMTD
5, 3079–3115, 2012

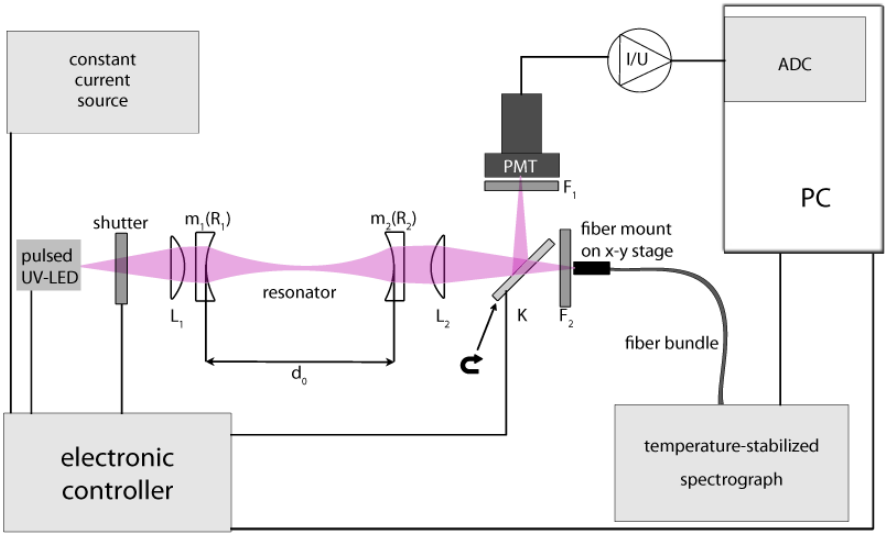

Fig. 1. Schematic diagram of the CE-DOAS-instrument. The radiation output of a pulsed UV-LED is imaged by lens L_1 into the resonator consisting of two highly reflective dielectric mirrors m_1 and m_2. The light which leaves the resonator through m_2 is focused by the lens L_2 to a fiber bundle which is attached to a x-y stage. This fiber bundle transmits the light to a temperature stabilized spectrograph (Ocean Optics QE 65000). Alternatively the movable mirror "K" can redirect the light to a photomultiplier (PMT) to optionally record a ring down signal and thus check the quality (and thus path length) of the resonator (which may change e.g. due to contamination of the mirrors). F_1 and F_2 are band-pass filters. F_1 protects the PMT and F_2 the fibers from scattered light and LED radiation outside of the reflectivity range of the mirrors. The shutter is used to perform background measurements. The electronic controller receives a constant current and creates the pulses for the UV-LED. It also controls the shutter and the mirror K.

AMTD
5, 3079–3115, 2012

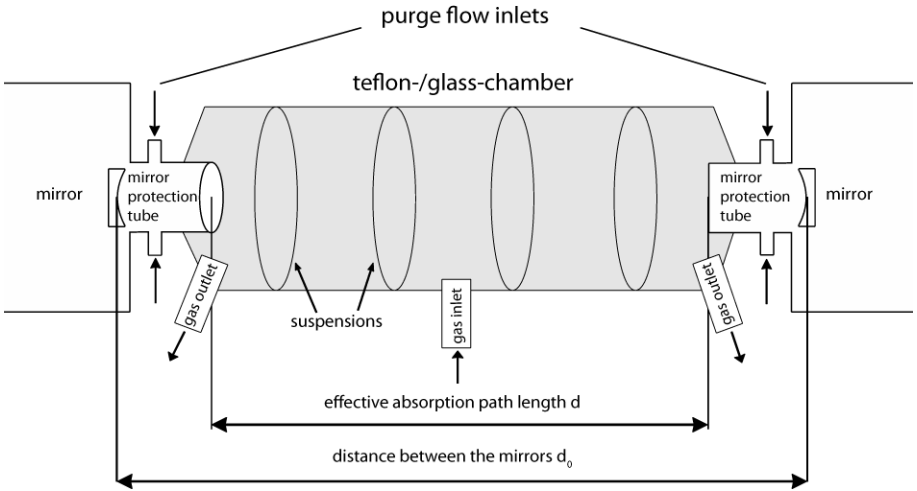

Fig. 2. Setup for the measurements at the Atmospheric Chemistry Research Laboratory, University of Bayreuth, Germany. One of three air tight chamber, made of either teflon or glass, is placed between the two mirrors. This chamber could be filled via the gas inlet with different trace gases. A purge flow of nitrogen in front of the mirrors avoids aerosols from the sample air to contaminate the mirrors. The distance between the mirrors is d_0. The effective absorption path length is d because the sample gas only fills the volume between the ends of the mirror protection tubes between the purge gas outlets.

AMTD
5, 3079–3115, 2012

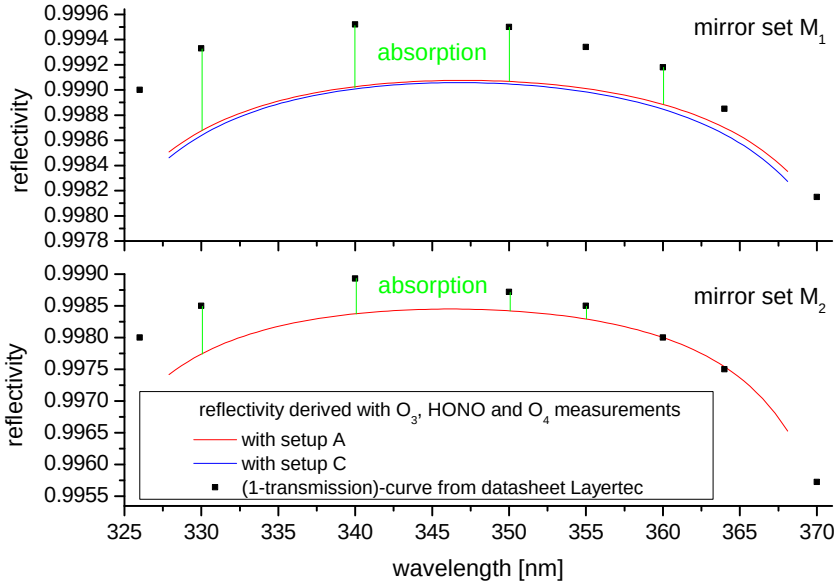

Fig. 3. Reflectivity curves of mirror sets M_1 and M_2: the black squares indicate the (1-transmission)-curve from the manufacturer's data sheet. The red and blue lines are the reflectivities calculated from measurements with setup A and C respectively. The green lines between the black dots and the reflectivity-curves indicate the losses due to absorption in the reflective layer. It can be seen that the absorption is very small at 370 nm and increases towards shorter wavelengths.

AMTD
5, 3079–3115, 2012

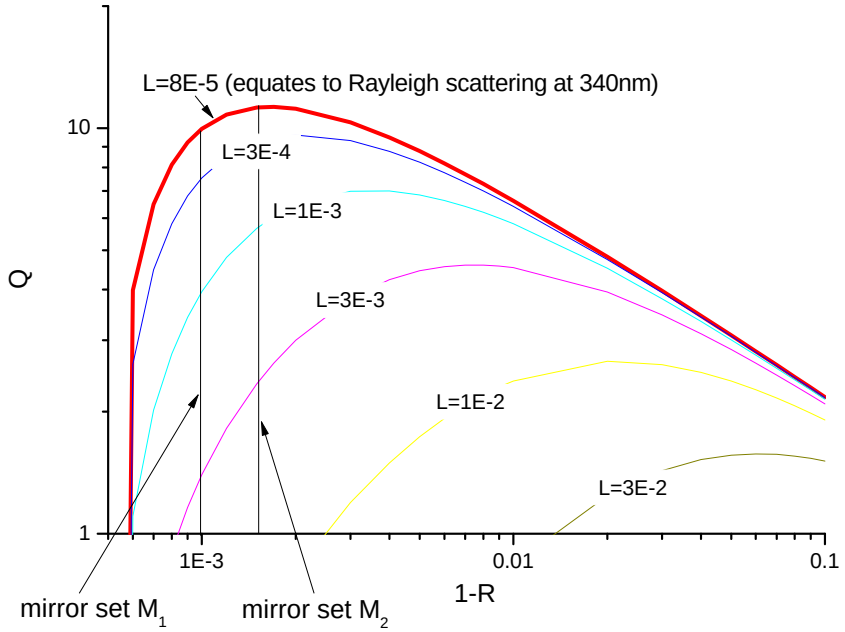

Fig. 4. Calculation of the enhancement factor (quality factor) Q from Eq. (12) (Fiedler et al., 2007) as a function of $(1 - R)$ for different losses L and a mirror absorption $A = 4 \times 10^{-4}$. The red line indicates upper limit for Q for the minimal losses due to Rayleigh scattering in the resonator at 340 nm.

AMTD
5, 3079–3115, 2012

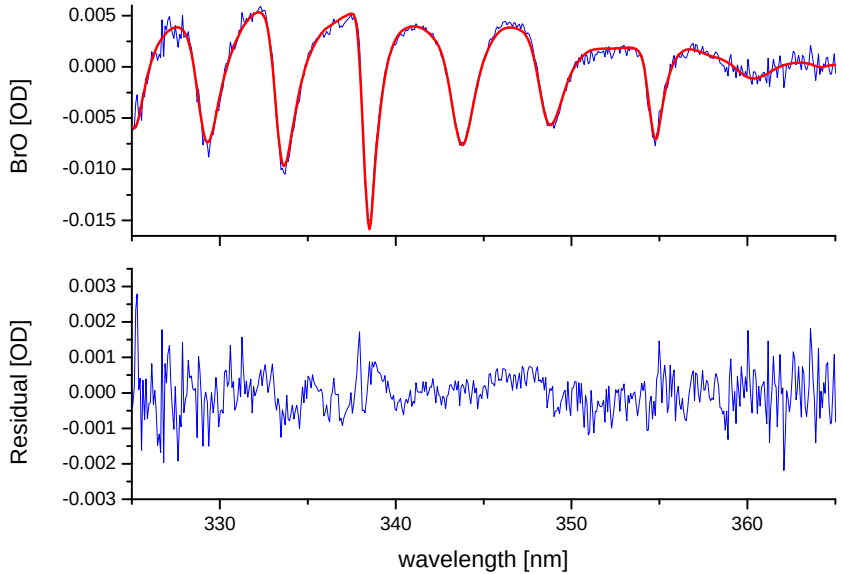

Fig. 5. Spectral DOAS fit of BrO with (507 ± 11) ppt. Upper panel: the thick red line indicates the fit result and the thin blue line the sum of the fit result and the residual. Lower panel: fit residual.

AMTD
5, 3079–3115, 2012

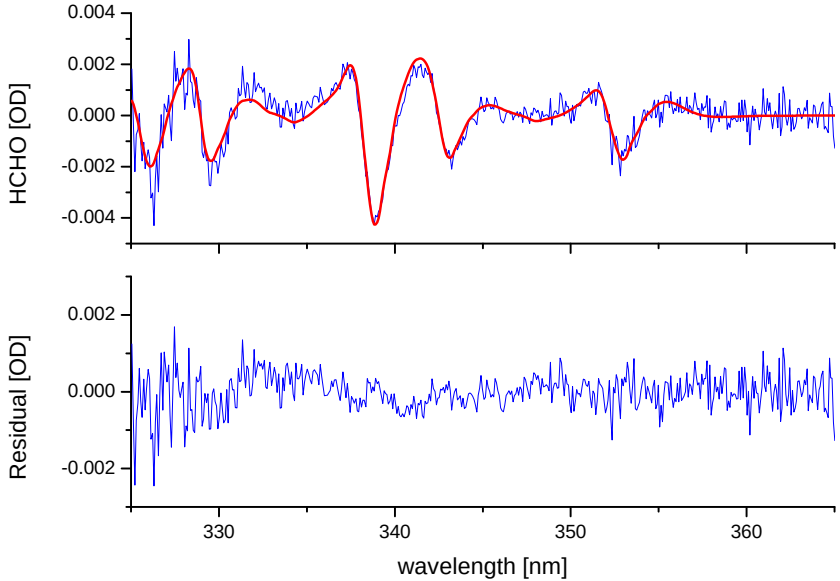

Fig. 6. Spectral DOAS fit of HCHO with (88 ± 6) ppb. Upper panel: the thick red line indicates the fit result and the thin blue line the sum of the fit result and the residual. Lower panel: fit residual.

AMTD
5, 3079–3115, 2012

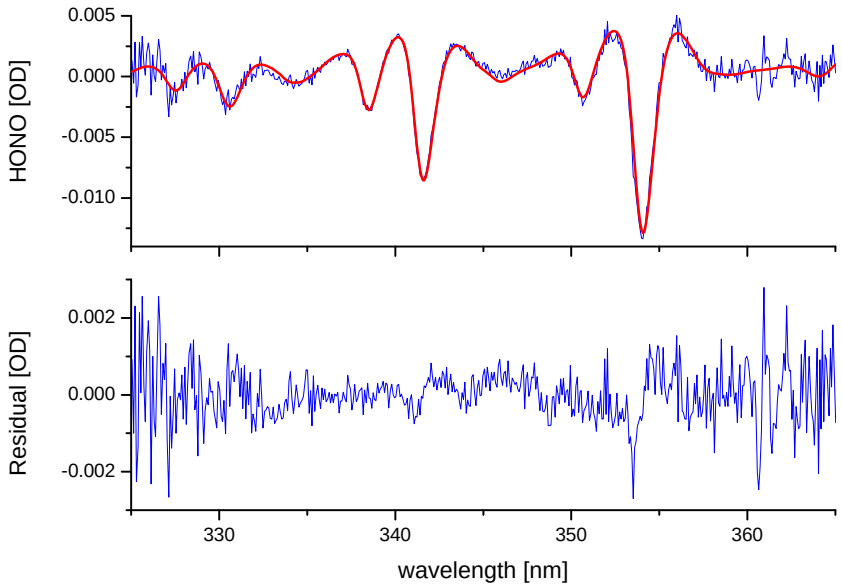

Fig. 7. Spectral DOAS fit of HONO with (16.0 ± 0.7) ppb. Upper panel: the thick red line indicates the fit result and the blue thin line the sum of the fit result and the residual. Lower panel: fit residual.

AMTD
5, 3079–3115, 2012

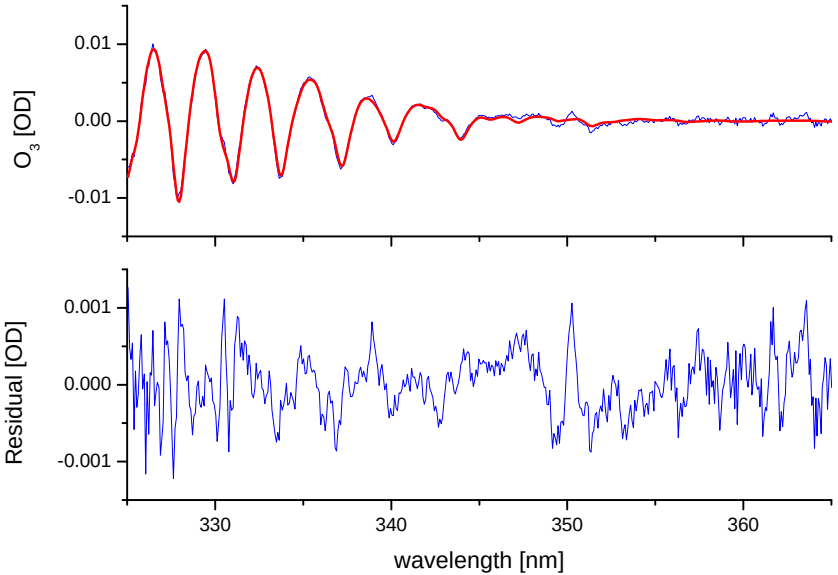

Fig. 8. Spectral DOAS fit of O_3 with (1766 ± 59) ppb. Upper panel: the thick red line indicates the fit result and the thin blue line the sum of the fit result and the residual. Lower panel: fit residual.

AMTD
5, 3079–3115, 2012